Mammographic Image Classification Based on KAN-CBAM

Yuanyuan Wang[1], Vladimir Mariano[2]
College of Computing and Information Technologies, National University, Manila, Philippines[1, 2]
School of Information Engineering, Guizhou University of Traditional Medicine, Guizhou, China[1]

***Abstract*—With the fast enhancement of deep learning, research on automatic detection of breast tumors is becoming increasingly in-depth. However, traditional CNNs' linear kernel has difficulty not only in capturing the nonlinear combination of low-frequency structures and high-frequency details but also in fully exploring the nonlinear discriminative features in medical images. Furthermore, the current models used for breast tumor detection have complex structures and slow inference speeds. Therefore, this study solves the linear kernel problem and improves the model inference speed by using a lightweight mammographic image classification method based on KAN-CBAM to speed up breast cancer diagnosis. The proposed method introduces the KAN convolution module, which embeds a learnable B-spline activation function into the convolution kernel. This scheme improves the capability of the proposed method to capture nonlinear features and improves its capacity to fit complex, nonlinear distributions. Moreover, the proposed method combines the CBAM attention mechanism to screen key semantic channels through channel attention and then uses spatial attention to locate lesion areas, achieving "channel-space" dual feature recalibration, further improving the attention to key features, and achieving more accurate classification in complex and variable medical images. We evaluated the proposed method on the mammographic image datasets DDSM, INbreast, and MIAS to verify its performance. The results prove that KAN-CBAM models have higher adaptation to diverse dataset scales, efficiently acquiring major lesion parts and nonlinear discriminatory features in mammographic images. Meaningful and great enhancements were seen in different metrics such as accuracy, F1-score, AUC, precision, and recall, demonstrating extensively improved model strength and generalization capability.**

Keywords*—KAN; CBAM; deep learning; mammographic; classification

I. Introduction

A. Background of the Study

Breast cancer is one of the most common female fatal tumors characterized by abnormal proliferation of breast tissue and tumor formation. Its incidence rate exceeds even that of lung cancer, becoming the world's largest cancer [1][2]. Timely diagnosis of benign and malignant breast tumors allows for earlier treatment, thereby reducing patients' life risk and helping to decrease breast cancer mortality [3]. Therefore, the recognition of breast tumors is crucial to the judgment of breast cancer. Common breast imaging techniques include HP (Histo-Pathology), US (Ultrasound), MRI (Magnetic Resonance Imaging), DM (Digital Mammography), and mammography images [4], which serve important roles in the early identification of malignant lesions.

Currently, mammography is the only imaging modality widely recognized as suitable for large-scale screening of asymptomatic women and serves as the cornerstone of breast-cancer screening programs worldwide [5]. Because of its low cost and medical requirements, it has become one of the most widely used detection methods for breast cancer diagnosis [6]. In the context of breast cancer, a large number of researchers are committed to exploring strategies for classifying benign and malignant tumors [7]. In order to better detect and diagnose breast cancer cases on time, deep learning (DL) technology is a promising method for disease detection in the medical field. Compared with traditional image classification models such as Support Vector Machine (SVM) [8], Fuzzy Cognitive Map (FCM) [9], or Multi-Layer Perceptron (MLP) [10], deep learning techniques can automatically discover features in breast images that contain benign and malignant discrimination information, and have stronger breast feature extraction capabilities, such as convolutional neural networks (CNN) [11], which demonstrate powerful capabilities in image feature extraction. Based on CNN, various types of image classification models were constructed based on different learning algorithms [12]. Jafari, Z. et al. [13] proposed a CNN model based on feature extraction and dimensionality reduction for breast cancer detection in mammography images. According to the results, the method achieved better classification accuracy. Bouzar Benlab, L. et al. [14] proposed a new framework for breast cancer detection of breast X-ray images, called the CNN-CBR classification system. In order to improve the accuracy of CBR, the authors implemented image enhancement and data enhancement to optimize the effect of feature extraction. Efficiently obtaining regions of interest (ROI) in breast images through the U-Net architecture, this framework combines deep learning (DL) with CBR. Deep learning helps achieve accurate breast image segmentation, while CBR provides interpretable and accurate classification results. S. Majumdar et al. [15] combined three transfer CNN models, namely GoogleNet, VGG11, and MobileNetV3_Small, to solve the binary classification problem of breast tissue pathology images using the Gamma function. Moreover, J. G., T. Melekoodapattu et al. [16] designed an automatic diagnosis system for breast cancer. The system uses a CNN containing nine convolution layers to extract image texture features and then classify the extracted features. When extracting image-texture features, we reduce the dimension of breast-image representations layer by layer, thereby enhancing the expressiveness of the learned features and improving

breast-cancer diagnostic accuracy. In general, with CNN as the core, the automatic recognition accuracy and robustness of breast cancer images have been significantly improved through feature engineering, data enhancement, transfer learning, or fusion with traditional machine learning and other strategies.

Even though CNN-based image-feature techniques have achieved strong performance in medical imaging, the lesion regions in medical images exhibit highly complex characteristics. Existing neural networks based on fully connected layers still cannot solve the linear kernels problem, that is, the network has no perception in the spatial dimension and lacks nonlinear activation. The overall degradation is linear mapping, making it difficult to capture complex textures and deep semantics, and making it unable to effectively handle nonlinear classification problems of medical image data [17]. For this reason, the Kolmogorov-Arnold Network (KAN) has been applied to image-processing tasks [18]. Shi, Y et al. [19] have successfully integrated the U-KAN and C-KAN frameworks to address the challenge of medical image segmentation, accurately delineating anatomical structures and lesion areas, and providing a core basis for clinical decision-making. Omid Nejati Manzari et al. [20] embedded the KAN layer into Transformer to form a new framework and then proposed an enhanced Dilated Neighborhood Attention (DiNA) to achieve generalized medical image classification. Jianyun Liu et al. [21] devised a multi-scale feature-prediction network that first extracts feature maps via convolution, refines them with spatial attention, and finally sums the channels in a learnable Kolmogorov-Arnold layer to perform image classification.

B. Problem Statement

In the area of image processing, deep learning possesses substantial benefits, but the mainstream methods still have certain problems, mainly manifested as follows.

1) For CNN models, gradient degradation is prone to occur when the network deepens, making it difficult to fully capture global contextual information, and many model structures are complex.

2) CNNs can only represent linear mappings and are insensitive to higher-order statistics and texture information. In mammograms, however, malignant signs often manifest as higher-order distributions of texture and micro-calcification clusters. Relying solely on linear mappings makes it difficult to encode such high-order information into feature maps; additional nonlinear activations, pooling, or subsequent fully connected layers are required to partially compensate.

3) KAN adopts a fully connected topology, which has insufficient utilization of local priors in two-dimensional images and lacks spatial induction bias.

C. Objectives

To tackle these problems, this study proposes a KAN architecture enhanced with the Convolutional Block Attention Module (CBAM) [22] that successfully performs a three-class classification: benign, malignant, and normal. The main objectives are:

1) Introducing lightweight model(s) specifically designed for the classification of mammographic images is proposed.

2) Replacing the linear convolution kernels of traditional CNNs with KAN convolution kernels upgrades "fixed-weight linear filtering" to "nonlinear weight generation driven by learnable activation functions". This allows the model to conduct higher-order mapping modeling within convolution layers without increasing or even reducing the parameter scale, eliminating the parameter and computation explosion caused by subsequent stacking of multi-layer nonlinear activations and redundant channels.

3) Incorporating the CBAM technique into the convolutional layers based on KAN to build a new architecture, which is capable of adapting prominent regions in the images, efficiently reducing noise, extracting key local features, having faster convergence, and enhancing stability and accuracy.

This study integrates the advantages of the CBAM technique into the advantages of KAN-based models to build fusion models that inherit high feature extraction and strong interpretability, presenting successive architectures in the field of classification on mammography images. The new models are capable of adapting to images having different qualities, remarkably when facing images that are noisy and have low resolution, it still presents high accuracy and stability.

II. Related Studies

The proposed method embeds KAN's learnable univariate activation functions into the convolutional layer, instantiating nonlinear weights within the channel dimension to overcome the spatial insensitivity and limited expressiveness of conventional "linear kernels". CBAM further jointly produces attention coefficients across both channel and spatial axes, precisely highlighting diminutive lesions while suppressing background redundancy, thereby markedly elevating diagnostic accuracy and interpretability for mammographic images.

A. KAN

Kolmogorov-Arnold Network (KAN) equips each edge with a learnable activation function in place of conventional weights. Rather than fixed linear weights, KAN replaces every parameter with a univariate spline function. According to the KAN representation theorem, every continuous multivariate mapping can be decomposed into a collection of one-dimensional functions, as shown in Eq. (1):

$$f(X) = f(x_1, \ldots\ldots, x_n) = \sum_{q=1}^{2n+1} \phi_q \left(\sum_{p=1}^{n} \emptyset_{q,p}(x_p) \right) \quad (1)$$

In a sense, they proved that the only true multivariate function is addition, because all other functions can be expressed through unary functions and summation operations. In a KAN, for a supervised-learning task made up of input-output pairs $\{x_i, y_i\}$, finding a function f so that y_i is approximately equal to $f(x_i)$ for each data point. The crux is to discover the appropriate univariate functions, inner (encoders) and outer (decoders); the architecture is shown in Fig. 1 (in the Appendix) [23].

Every learnable nonlinear function is univariate, taking only one input. It is modeled as a B-spline curve ϕ(x) whose local-basis coefficients c_i are learnable. In KAN, unlike traditional MLP, the weight of each connection in KAN is no longer a simple numerical value but is parameterized as a learnable spline function. By representing ∅_(q,p) and ϕ_q through B-splines and composing these functions, the entire network is constructed.

Overall, KAN, as a novel neural-network architecture, has demonstrated remarkable advantages both theoretically and experimentally, especially in accuracy, parameter efficiency, and interpretability.

B. CBAM

The Convolutional Block Attention Module (CBAM) is a simple and effective feedforward convolutional neural network attention module, which is commonly used for embedded int CNN to enhance the feature extraction capabilities from images. Given an intermediate feature map, the module infers the attention of the image along two independent dimensions, channel and space, and then multiplies the attention map by the input feature map for adaptive feature refinement [24][25][26][27][28]. CBAM is a lightweight universal module that can be well integrated into the KAN architecture presented in this article, with negligible overhead. This attention mechanism amplifies salient features while suppressing irrelevant ones.

Fig. 2 (in the Appendix) presents the architecture of the CBAM technique. As seen in this architecture, CBAM comprises two independent segments: CAM (Channel Attention Module) and SAM (Spatial Attention Module). Given an input feature map $F \in R^{(C\times H\times W)}$, CBAM sequentially produces a 1-D channel-attention $M_c \in R^{(C\times 1\times 1)}$, and a 2-D spatial-attention map $M_s \in R^{(1\times H\times W)}$ [29]. The overall attention procedure is summarized in Eq. (2) and (3) [30]. The ultimate output of CBAM is acquired by multiplying the result of the channel attention output by the weight of spatial attention.

$$F' = M_c(F) \otimes F \tag{2}$$

$$F'' = M_s(F') \otimes F' \tag{3}$$

1) CAM: Chanel Attention Module (CAM) at the first step squeezes the spatial axes of the feature map and then models cross-channel dependencies to deliver a channel-attention map. For the aggregation of spatial information, it adopts two types of pooling: max-pooling and average-pooling, which greatly improve the network's expressive power. CAM first gathers the three-dimensional information of the feature map via average-pooling and max-pooling, producing two distinct spatial-context descriptors, F^c_{avg} and F^c_{max}. These summaries are then fed to a single Multilayer Perceptron (MLP) subnet that outputs the channel-attention map $M_c \in \{\mathbb{R}^{c\times 1\times 1}\}$. The equation for calculating CAM is presented in Eq. (4) [26]. σ represents the Sigmoid function, W_0 represents the dimensionality reduction weight matrix with a shape of (c/r)×c, and W_1 represents the dimensionality enhancement weight matrix with a shape of c×(c/r), where r is considered the rate of reduction and the default value is 16.

$$\begin{aligned} M_c(F) &= \sigma(MLP(AvgPool(F) + MLP(MaxPool(F))) \\ &= \sigma(W_1(W_0(F^c_{avg})) + W_1(W_0(F^c_{max}))) \end{aligned} \tag{4}$$

2) SAM: Spatial Attention Module (SAM) multiplies CAM's channel attention by the input feature map to get SAM's input feature map. Spatial attention is different from channel attention, as it focuses on the type of information within a Feature Map and complements channel attention. Use two *channel=c* pooling operations to aggregate the channel information of feature maps, generating two 2-D feature maps. Each feature map aggregates channel information, representing the average and max-pooling characteristics across channels. Then use a standard convolutional layer to connect and convolve them to generate a 2-D spatial attention map, with the calculation shown in Eq. (5).

$$\begin{aligned} M_s(F) &= \sigma(f^{7\times 7}([AvgPool(F); MaxPool(F)])) \\ &= \sigma(f^{7\times 7}([F^s_{avg}; F^s_{max}])) \end{aligned} \tag{5}$$

Finally, a 7×7 convolution is applied to produce the spatial-attention matrix. Then, the sigmoid function converts the response map into spatial-attention weights, called the spatial attention map $M_s(F)$. Finally, the input feature map with the channel attention mechanism is element-wise multiplied by the output $M_s(F)$ to obtain the result of CBAM.

III. Methodology

This study proposes a lightweight model for mammographic image classification based on KAN-CBAM. By leveraging KAN, the network overcomes the nonlinear-classification bottlenecks of image processing while remaining highly interpretable. To further enhance feature extraction, we embed the CBAM attention mechanism inside every KAN convolutional layer, which not only helps the model converge faster but also helps extract more useful image features, focus on discriminative features, and make classification more accurate. Fig. 3 (in the Appendix) illustrates the overall architecture of KAN-CBAM.

The proposed framework is a convolutional neural architecture that combines the KAN and CBAM mechanisms. It consists of two convolutional blocks (Conv Block) and one classifier. Each Conv Block performs two key operations, namely KAN convolution and CBAM. The result from Conv Block 1 is channeled into Conv Block 2 through a residual connection, which helps address the vanishing gradient problem in deep networks and enhances the integrity of feature propagation. Finally, the Classifier module converts the extracted features into class probabilities via fully connected layers, batch normalization, and Dropout, completing the classification task.

Due to the introduction of KAN-enhanced feature extraction, combined with CBAM-enhanced feature selection and the use of residual learning to alleviate gradient degradation, the proposed model improved representation ability while reducing redundancy. Finally, it was validated on the dataset, achieving efficient and high-precision image classification.

A. KAN Convolution

According to Fig. 3, the KAN-Convolutional Layer is located in Conv Blocks. The KAN convolutional layer extracts features with its unique function approximation ability, providing more expressive initial feature maps for subsequent processing.

KAN convolution is a special convolution operation that applies a learnable nonlinear function to each edge and adds them together. Every weight is recast as a univariate spline function, and nodes merely add up the input signals without using nonlinear operations.

Traditional CNNs mainly depend on set activation functions and linear transformations to capture spatial relationships. Although this design effectively handles complex spatial data, it lacks sufficient flexibility and expressiveness. By directly replacing the nonlinear activation function of KANs in the convolutional layer, KAN convolutional layers can be constructed. KANs reduce the number of parameters and may improve generalization ability by introducing learnable spline functions, B-splines. This new layer type not only maintains the efficiency of CNN in processing image data but also enhances its flexibility and expressiveness through the spline function of KANs.

In KAN convolution, the spline is constructed primarily from B-spline basis functions, as given in Eq. (6), where $B_i(x)$ represents a B-spline basis function, and c_i is a learnable coefficient that controls the weights of the basis functions. The spline is constructed by linearly combining multiple local basis functions, and the parameters that KAN truly needs to learn are the coefficients c_i in front of the basis functions. By adjusting the parameters of the spline, it can adapt to different data distributions and task requirements.

$$spline(x) = \sum_{i=1}^{n} c_i \cdot B_i \quad (6)$$

B. KAN-CBAM Model

To enhance the automatic focusing ability of KAN convolutional layers on discriminative regions and channels, the model inserts the Convolutional Block Attention Module (CBAM) after KAN convolution to form KANConv-CBAM units. CBAM applies channel and spatial dimension attention weighting to the feature maps of channels 4 and 8, respectively, highlighting key features, suppressing irrelevant information, and enhancing the effectiveness of feature expression.

The channel attention structure is shown in Fig. 4 (in the Appendix), which chiefly employs channel management among features to create channel attention maps. In the module, the input feature map F, which has dimensions of C×H×W, experiences both global max-pooling and global average-pooling operations. Specifically, global max-pooling is carried out along the W dimension, while global average-pooling is performed along the H dimension. Consequently, two feature maps with dimensions of C×1×1 are acquired. These maps are subsequently input into a 2-layer MLP, in which the output features are aggregated and sigmoid-activated to produce the final feature.

The architecture of the spatial attention module is shown in Fig. 5 (in Appendix), which generates a spatial attention map using the spatial relationships between features, focusing on where the information is located. This module utilizes the feature map, which is the output of the Channel Attention Module, as its input. The feature map undergoes average-pooling and max-pooling operations to obtain two feature maps. Next, the two feature maps are merged in the channel dimension and connected and convolved using a standard convolution layer to obtain a 2-dimensional spatial attention map. Finally, the sigmoid function is used to achieve spatial attention features.

This spatial attention map reflects the importance of different spatial positions in the feature map. It is then element-wise multiplied by the channel-attended feature map, spatially re-weighting the activations so that salient locations are emphasized.

IV. Results and Discussion

This section first introduces the datasets and then presents the experiment parameters. Ultimately, the results of the experiment are compared and analyzed to confirm the effectiveness of the algorithm proposed in this study.

A. Datasets

This study mainly selects to validate the model using the public datasets: DDSM, which includes 5,238 images, INbreast, which includes 13,172 images, and MIAS, which includes 322 images. These datasets are mainly divided into three categories: normal, benign, and malignant. Each dataset was partitioned with an 80/20 split for training and testing.

Through analysis of the datasets, it is known that there are many images with inconsistent resolutions, noise interference, and significant differences in image size and shape, as shown in Fig. 6 (a),(b), and(c) (in Appendix). However, the proposed method effectively overcomes these problems in the dataset and efficiently completes the image classification task.

B. Experimental Environment

To verify the effectiveness of this project, validation was conducted on a laptop computer and in the hardware environment as listed in Table I.

TABLE I. Hardware Environment Parameters

Hardware	Parameters
GPU	NVIDIA T600
RAM	32.0 GB
Storage	2TB
CPU	Intel Core i7-11700 @ 2.50GHz

C. Experimental Results

1) Major metrics comparison: This study primarily employs accuracy, loss, F1-score, Recall, and AUC as major evaluation metrics to verify the performance of the model. It mainly compares the classification performance of seven KAN-based models and KAN-CBAM models enhanced with the CBAM. Table VI (in the Appendix) presents the

classification results of the seven KAN-based models, while Table VII (in the Appendix) shows those of the seven KAN-CBAM models. In the tables, "M" stands for Medium, "B" stands for Big, and "S" stands for Small.

Experimental results in Table VI and Table VII (in the Appendix) indicate KAN-CBAM-based models exhibit superior performance – especially regarding accuracy, F1 score and AUC – compared to KAN-based models among the three datasets.

On the DDSM dataset, in KAN-CBAM-based models, KANC MLP (B) is the superior model, presenting values 84.85%, 84.01%, and 85.87% regarding accuracy, F1-score, and AUC, respectively, while in KAN-based models, KKAN (M)is the superior model, showing values 84.04%, 83.09%, and 84.15%.

On the INbreast dataset, in KAN-CBAM-based models, KKAN (M) is the superior model, presenting values of 99.66%, 99.64%, and 99.70% regarding accuracy, F1-score, and AUC, respectively. In KAN-based models, KANC MLP (B) is the superior model for accuracy and F1-score, showing values 98.90% and 98.82%, respectively, while KANC MLP (M) is the superior model for AUC, having a value of 99.62%.

On the MIAS dataset, in KAN-CBAM-based models, KKAN (S) is the superior model regarding accuracy and AUC, having values of 85.00% and 79.21%, respectively, and KANC MLP (M) is the superior model regarding F1-score, having a value of 83.33%. In KAN-based models, KKAN (S) is the superior regarding accuracy, F1-score, and AUC, having values of 75.00%, 49.36%, and 59.21%, respectively.

2) AUC comparison: To evaluate the effect of the CBAM technique on the KAN-based models, AUC values of all KAN-based models were compared with corresponding KAN-CBAM-based models for DDSM, INbreast, and MIAS datasets separately. Fig. 7 (in Appendix), Fig. 8 (in Appendix), and Fig. 9 (in Appendix) present AUC comparison on DDSM, INbreast, and MIAS datasets, respectively.

As Fig. 7 shows, for the DDSM dataset, generally, KAN-CBAM-based models accomplished higher AUC values compared to KAN-based models. The most enhancement was for the KANC (M) model, in which the AUC value increased from 51.27% to 81.13%, introducing a strong improvement in discriminative potential after integrating the CBAM technique. Further enhancements were also seen for KAN (M), KAN (S), KANC (B), KANC (S), and KKAN (S). Only KKAN (M) presented a trivial reduction in AUC.

For INbreast dataset, KAN-based models and KAN-CBAM-based models both made high AUC values, signaling that this dataset is extremely separable for most models. Therefore, the differences in AUC values between KAN-based models and KAN-CBAM-based models are quite small.

For the MIAS dataset, the contribution of the CBAM technique was the brightest, since all KAN-CBAM-based models overtook their relevant KAN-based models. The largest increases in AUC were seen in KANC (B), KANC (S), KKAN (M), and KKAN(S), indicating that the CBAM technique affected highly feature enhancement and class discrimination on this dataset.

Taken together, AUC analysis shows that generally the CBAM technique enhances discriminative performance, with the highest effect seen on the MIAS dataset, followed by the DDSM dataset, while on INbreast dataset, the contribution of CBAM is trivial due to the existence of high reference performance.

3) Loss comparison: A comparison was performed over loss values of KAN-based models and KAN-CBAM-based models, since smaller loss indicates better optimization behavior. Fig. 10 (in Appendix), Fig. 11 (in Appendix), and Fig. 12 (in Appendix) present the loss comparison of DDSM, INbreast, and MIAS datasets, respectively.

For the DDSM dataset, generally, KAN-CBAM-based models present lower loss values compared to relevant KAN-based models. The largest reduction was seen for KANC (M), in which the loss value dropped from a value of 0.0291 to a value of 0.0115. Another large reduction was seen for KKAN (M), in which the loss decreased from a value of 0.0118 to a value of 0.0030.

For INbreast dataset, KAN (M), KAN (S), and KANK (S) introduced slightly lower loss values without the CBAM technique, while KANC (M) showed a large improvement after the incorporation of the CBAM technique. For the remaining models, the differences were trivial or zero.

For the MIAS dataset, the effect of the CBAM technique was not consistent. A small reduction was seen for KAN (M), whereas KKAN (M and KKAN (S) persisted unchanged. All other models presented trivial growth in loss value after the integration of the CBAM technique. This specifies that the effect of CBAM on loss optimization is architecture-dependent.

Overall, loss analysis shows that the CBAM technique presents the strongest optimization on the DDSM dataset, while its effect on INbreast and MIAS datasets is not consistent and depends on model configuration.

4) Other metrics comparison: Precision, specificity, and Matthew Correlation Coefficient (MCC) capture complementary aspects and attributes of analytical reliability which are not exhibited by accuracy, F1-score, recall, AUC, and loss.

Precision is important since it shows the ratio of predicted positive samples that are truly identified as positive. In this study, greater precision shows smaller false positive predictions, thus helping decrease unnecessary follow-up tests and patient fear and anxiety.

Specificity shows the ratio of predicted negative samples that are truly negative, indicating the model's capability to prevent falsely classifying normal cases or benign cases as abnormal.

MCC presents a well-adjusted summary of the performance of the classification by considering four parameters in the confusion matrix: true positive, false positive, true negative,

and false negative. The summary presented by MCC is helpful when a complete view of the reliability of a model in classification is needed.

To prevent an extremely long presentation, precision, specificity, and MCC are summarized as average values shown in Table II.

As Table II shows, generally, KAN-CBAM-based models attain larger average values than KAN-based models within all three metrics (precision, specificity, and MCC) across all datasets. This supports the idea that the integration of the CBAM technique not only enhances discrimination performance but also increases the reliability of the classification.

5) Delta analysis: To have a better numerical understanding of the effect of the CBAM technique, the absolute changes between each KAN-based model and the corresponding KAN-CBAM-based model were computed for AUC and loss. It should be noted that a positive value for ΔAUC means that the CBAM technique enhanced discriminative performance, while a negative value for ΔLoss means that the CBAM technique lowered the loss value, hence enhancing optimization behavior. Tables III, IV, and V present absolute changes after the inclusion of the CBAM technique on DDSM, INbreast, and MIAS datasets, respectively.

The values in the delta analysis support the values in the bar charts presented earlier. On the DDSM dataset, the CBAM technique enhances most models, while the largest benefit is seen for KANC (M). On INbreast dataset, the contribution of CBAM was minor and somewhat mixed, which is likely associated with the high existing performance of KAN-based models. On the MIAS dataset, all models gained from the CBAM technique in terms of AUC, implying a consistent positive effect of architecture-based feature enhancement on this dataset.

The values related to ΔLoss also prove that enhancements in AUC are not always consistent with reductions in loss. For instance, CBAM showed a large loss reduction on the DDSM dataset, whereas its effect on MIAS and INbreast datasets was dependent on the model's architecture. This proposes that the contribution of the CBAM technique is not solely optimization-driven but also relevant to how successfully the attention process improves discriminative feature interpretation.

TABLE II. SUMMARY OF PRECISION, SPECIFICITY, AND MCC

Dataset (Model based)	Avg. Precision	Avg. Specificity	Avg. MCC
DDSM (KAN)	0.734	0.747	0.484
DDSM (KAN-CBAM)	0.800	0.813	0.604
INbreast (KAN)	0.876	0.969	0.864
INbreast (KAN-CBAM)	0.974	0.989	0.970
MIAS (KAN)	0.414	0.553	0.141
MIAS (KAN-CBAM)	0.813	0.831	0.616

TABLE III. ABSOLUTE CHANGE AFTER CBAM INTEGRATION ON DDSM DATASET

Model Pair	ΔAUC	ΔLoss
Conv & KAN (M)	+0.0712	-0.0009
Conv & KAN (S)	+0.0308	-0.0005
KANC MLP (B)	+0.0358	-0.0006
KANC MLP (M)	+0.2986	-0.0176
KANC MLP (S)	+0.0466	-0.0013
KKAN (M)	-0.0036	-0.0088
KKAN (S)	+0.0134	-0.0004

TABLE IV. ABSOLUTE CHANGE AFTER CBAM INTEGRATION ON INBREAST DATASET

Model Pair	ΔAUC	ΔLoss
Conv & KAN (M)	-0.0173	+0.0124
Conv & KAN (S)	-0.0305	+0.0167
KANC MLP (B)	+0.0002	+0.0001
KANC MLP (M)	-0.0017	-0.0004
KANC MLP (S)	+0.0236	+0.0005
KKAN (M)	+0.0314	+0.0009
KKAN (S)	+0.0219	+0.0015

TABLE V. ABSOLUTE CHANGE AFTER CBAM INTEGRATION ON MIAS DATASET

Model Pair	ΔAUC	ΔLoss
Conv & KAN (M)	+0.2093	-0.0037
Conv & KAN (S)	+0.1916	+0.0040
KANC MLP (B)	+0.2836	+0.0033
KANC MLP (M)	+0.1882	+0.0005
KANC MLP (S)	+0.2296	+0.0042
KKAN (M)	+0.2000	+0.0000
KKAN (S)	+0.2000	+0.0000

D. Summary of Performance Indicators

The results show that the inclusion of the CBAM technique generally enhances KAN-based models' performance within the datasets considered. This matter is strongly confirmed not only by AUC, loss, and delta analyses, but also by other metrics such as precision, specificity, and MCC. Overall, the findings denote that the CBAM technique offers not only higher discriminative capability but also greater enhancement in classification reliability.

V. CONCLUSION AND FUTURE WORKS

This study worked on the effect of the CBAM technique by comparing KAN-based and KAN-CBAM-based models on the three datasets – DDMS, INbreast, and MIAS – including breast cancer images.

The results indicated that incorporating the CBAM technique enhances performance, especially regarding AUC, in which the most consistent benefits were seen on the MIAS

dataset, and high enhancement was found on the DDSM dataset, whereas the improvement was trivial on INbreast dataset, since most of the models already attained very high performance.

Based on the results of the loss analysis, the contribution of the CBAM technique to optimization likely depends on the architecture and the dataset. The highest loss reduction was seen on the DDSM dataset, whereas the impacts on the MIAS and INbreast datasets were mixed. Moreover, the results regarding precision, specificity, and MCC confirmed the advantage of integrating CBAM into the models studied.

In future studies, the models studied can be assessed under other testing settings and on other medical datasets. In addition, future studies can integrate robustness analysis and statistical significance testing over explanatory models to have a better evaluation of CBAM and its effects.

REFERENCES

[1] https://who.int/news-room/fact-sheets/detail/breast-cancer, Accessed on: January 6, 2026.

[2] http://www.52qixiang.com/info/83134.html, Accessed on: January 6, 2026.

[3] S. K. Biswas and D. P. Mukherjee, "Recognizing architectural distortion in mammogram: A multiscale texture modeling approach with GMM," IEEE Trans. Biomed. Eng., vol. 58, no. 7, pp. 2023-2030, July 2011, DOI: 10.1109/TBME.2011.2128870

[4] L. Balkenende, J. Teuwen, and R. M. Mann, "Application of deep learning in breast cancer imaging," Seminars in Nuclear Medicine, vol. 52, no. 5, pp. 584-596. March 2022, DOI: 10.1053/j.semnuclmed.2022.02.003

[5] S. H. Heywang-Köbrunner, A. Hacker, and S. Sedlacek, "Advantages and disadvantages of mammography screening," Breast Care, vol. 6, no. 3, pp. 199–207, May 2011, DOI: 10.1159/000329005

[6] Z. Gandomkar and C. Mello-Thoms, "Visual search in breast imaging," Br. J. Radiol., vol. 92, no. 1102: 20190057, July 2019, DOI: 10.1259/bjr.20190057

[7] L. A. Aldakhil, H. F. Alhasson, S. S. Alharbi, R. U. Khan and A. M. Qamar, "Image-based breast cancer histopathology classification and diagnosis using deep learning approaches," Appl. Comput. Intell. Soft Comput., vol. 2025, Art. no. 7011984, February 2025, DOI: 10.1155/acis/7011984

[8] S. Islam et al., "Image processing and Support Vector Machine (SVM) for classifying environmental stress symptoms of pepper seedlings grown in a plant factory," Agronomy, vol. 14, no. 9, Art. no. 2043, September 2024, DOI: 10.3390/agronomy14092043

[9] M. Hosseinpour, S. Ghaemi, S. Khanmohammadi and S. Daneshvar, "A hybrid high-order type-2 FCM improved random forest classification method for breast cancer risk assessment," Appl. Math. Comput., vol. 424, p. 127038, July 2022, DOI: 0.1016/j.amc.2022.127038

[10] A. Igali and P. Shamoi, "Image classification using fuzzy pooling in convolutional Kolmogorov-Arnold networks," in SCIS & ISIS 2024, Himeji, Japan, 2024, pp. 1-7

[11] L. Alzubaidi et al., "Review of deep learning: Concepts, CNN architectures, challenges, applications, future directions," J. Big Data, vol. 8, no. 53, March 2021, DOI: 10.1186/s40537-021-00444-8

[12] S. Alam Ansari, A. P. Agrawal, M. A. Wajid, M. S. Wajid and A. Zafar, "MetaV: A pioneer in feature augmented meta-learning based vision transformer for medical image classification," Interdiscip. Sci. Comput. Life Sci., vol. 16, No. 2, pp. 469-488, June 2024, DOI: 10.1007/s12539-024-00630-1

[13] Z. Jafari and E. Karami, "Breast cancer detection in mammography images: A CNN-based approach with feature selection," Information, vol. 14, no. 7, 410, July 2023, DOI: doi.org/10.3390/info14070410

[14] L. Bouzar-Benlabiod, K. Harrar, L. Yamoun, M. Y. Khodja and M. A. Akhloufi "A novel breast cancer detection architecture based on a CNN-CBR system for mammogram classification," Comput. Biol. Med., vol. 163, p. 107133, June 2023, DOI: 10.1016/j.compbiomed.2023.107133

[15] S. Majumdar, P. Pramanik and R. Sarkar, "Gamma function based ensemble of CNN models for breast cancer detection in histopathology images," Expert Syst. Appl., vol. 213, Part B, 119022, March 2023, DOI: 10.1016/j.eswa.2022.119022

[16] J. G. Melekoodappattu, A. S. Dhas, B. K. Kandathil and K. S. Adarsh, "Breast cancer detection in mammogram: Combining modified CNN and texture feature based approach," J. Ambient Intell. Human. Comput., vol. 14, pp. 11397-11406, September 2023, DOI: 10.1007/s12652-022-03713-3

[17] J. Gao et al., "MSFKAN: A multi-scale feature prediction network combined with KAN for medical image classification," Neural Process. Lett., vol. 57, no. 67, July 2025, DOI: 10.1007/s11063-025-11782-6

[18] N. Firsov et al., "HyperKAN: Kolmogorov–Arnold networks make hyperspectral image classifiers smarter," Sensors, vol. 24, no. 23, 7683, November 2024, DOI:10.3390/s24237683

[19] Y. Shi, S. Jiang, X. Liu, Y. Gao and G. Xu, "U-CKAM based on C-KAN and MRF for medical image segmentation," in Data Inf. Online Environ. (DIONE 2024), Lect. Notes Inst. Comput. Sci., Soc. Inform. Telecommun. Eng., vol. 569, Springer, Cham, 2026, pp. 235-246, DOI: 10.1007/978-3-031-97352-9_19

[20] O. Nejati Manzari, H. Asgariandehkordi, T. Koleilat, Y. Xiao and H. Rivaz, "Medical image classification with KAN-integrated transformers and dilated neighborhood attention," Appl. Soft Comput., vol. 178, 114045, October 2025, DOI: 10.1016/j.asoc.2025.114045

[21] T. Liu, Y. Yu, M. Yang, Z. Xiao, Q. Li and Y. Tang, "LCTKAN: Lightweight convolution Transformer–KAN for medical image classification," Biomedical Signal Processing and Control, vol. 116, 109553, May 2026, DOI: 10.1016/j.bspc.2026.109553

[22] S. Woo, J. Park, J. Y. Lee, and I. S. Kweon, "CBAM: Convolutional block attention module," in ECCV, Lecture Notes in Computer Science, vol. 11211, Cham, Switzerland: Springer, 2018, pp. 3-19, DOI: 10.1007/978-3-030-01234-2_1

[23] Z. Liu et al., "KAN: Kolmogorov-Arnold networks," in Int. Conf. Learn. Representations (ICLR), vol. 2025, pp. 70367-70413

[24] S. Woo, J. Park, J. Y. Lee, and I. S. Kweon, "CBAM: Convolutional block attention module," in Eur. Conf. Comput. Vis. (ECCV), Munich, Germany, September 2018, pp.3-19, DOI: 10.1007/978-3-030-01234-2_1

[25] M. Zakariah and A. Alnuaim, "Recognizing human activities with the use of Convolutional Block Attention Module," Egyptian Informatics Journal, vol. 27, September 2024, 100536, DOI: 10.1016/j.eij.2024.100536

[26] J. Qin, S. Zhang, Y. Wang, F. Yang, X. Zhong and W. Lu, "Improved skeleton-based activity recognition using convolutional block attention module," Computers and Electrical Engineering, vol. 116, May 2024, 109231, DOI: 10.1016/j.compeleceng.2024.109231

[27] M. M. Farag, M. Fouad and A. T. Abdel-Hamid, "Automatic Severity Classification of Diabetic Retinopathy Based on DenseNet and Convolutional Block Attention Module," IEEE Access, vol. 10, pp. 38299-38308, 2022, DOI: 10.1109/ACCESS.2022.3165193

[28] S. Agac and O. D. Incel, "On the Use of a Convolutional Block Attention Module in Deep Learning-Based Human Activity Recognition with Motion Sensors," Diagnostics, vol. 13, no. 11, 1861, May 2023, DOI: 10.3390/diagnostics13111861

[29] P. Wen, et al. "A-PSPNet: A novel segmentation method of renal ultrasound image", IEEE International Conference on Systems, Man, and Cybernetics (SMC), October 2021, pp. 40-45, DOI: 10.1109/SMC52423.2021.9658740

[30] K. Zheng, D. Yang, J. Liu and J. Cui. "Recognition of teachers' facial expression intensity based on convolutional neural network and attention mechanism", IEEE Access, vol. 8, pp. 226437-226444, December 2020, DOI: 10.1109/ACCESS.2020.3046225

APPENDIX

TABLE VI. EXPERIMENTAL RESULTS OF KAN-BASED MODELS

Dataset	Evaluation metric	Conv & KAN (M)	Conv & KAN (S)	KANC MLP (B)	KANC MLP (M)	KANC MLP (S)	KKAN (M)	KKAN (S)
DDSM	Accuracy	0.7459	0.7125	0.8225	0.5132	0.8029	0.8404	0.8111
	Loss	0.0141	0.0152	0.0121	0.0291	0.0126	0.0118	0.0122
	F1-score	0.7075	0.6958	0.8193	0.5012	0.8016	0.8309	0.7996
	Recall	0.7226	0.7051	0.8202	0.5996	0.7916	0.8371	0.8103
	AUC	0.7011	0.6928	0.8229	0.5127	0.8023	0.8415	0.8105
INbreast	Accuracy	0.9620	0.9620	0.9890	0.9838	0.8368	0.8102	0.7443
	Loss	0.0001	0.0001	0.0005	0.0010	0.0001	0.0001	0.0001
	F1-score	0.9589	0.9589	0.9882	0.9825	0.8033	0.7649	0.6553
	Recall	0.9571	0.9571	0.9873	0.9796	0.7824	0.7460	0.6550
	AUC	0.9862	0.9862	0.9956	0.9962	0.9715	0.9656	0.9748
MIAS	Accuracy	0.7153	0.7307	0.7307	0.7307	0.7307	0.7307	0.7500
	Loss	0.0512	0.0435	0.0398	0.0387	0.0416	0.0378	0.0865
	F1-score	0.4089	0.4222	0.4222	0.4222	0.4222	0.4222	0.4936
	Recall	0.4762	0.5000	0.5000	0.5000	0.5000	0.5000	0.5357
	AUC	0.5218	0.5395	0.4586	0.5733	0.5000	0.5508	0.5921

TABLE VII. EXPERIMENTAL RESULTS OF KAN-CBAM-BASED MODELS

Dataset	Evaluation metrics	Conv & KAN (M)	Conv & KAN (S)	KANC MLP (B)	KANC MLP (M)	KANC MLP (S)	KKAN (M)	KKAN (S)
DDSM	Accuracy	0.8046	0.7769	0.8485	0.8339	0.8404	0.8371	0.8257
	Loss	0.0132	0.0147	0.0115	0.0115	0.0113	0.0030	0.0118
	F1-score	0.8013	0.7727	0.8401	0.8263	0.8339	0.8258	0.8241
	Recall	0.7916	0.7572	0.8503	0.8305	0.8471	0.8376	0.8227
	AUC	0.7723	0.7236	0.8587	0.8113	0.8489	0.8379	0.8239
INbreast	Accuracy	0.9821	0.9784	0.9886	0.9862	0.9914	0.9966	0.9924
	loss	0.0125	0.0168	0.0006	0.0006	0.0006	0.0010	0.0016
	F1-score	0.9359	0.9206	0.9877	0.9852	0.9908	0.9964	0.9918
	Recall	0.9219	0.9707	0.9883	0.9870	0.9916	0.9968	0.9913
	AUC	0.9689	0.9557	0.9958	0.9945	0.9951	0.9970	0.9967
MIAS	Accuracy	0.8076	0.8076	0.8230	0.8461	0.8153	0.8307	0.8500
	Loss	0.0475	0.0475	0.0431	0.0392	0.0458	0.0378	0.0865
	F1-score	0.7973	0.7973	0.8148	0.8333	0.8065	0.8222	0.7936
	Recall	0.7256	0.7256	0.7408	0.7642	0.7319	0.7521	0.7357
	AUC	0.7311	0.7311	0.7422	0.7615	0.7296	0.7508	0.7921

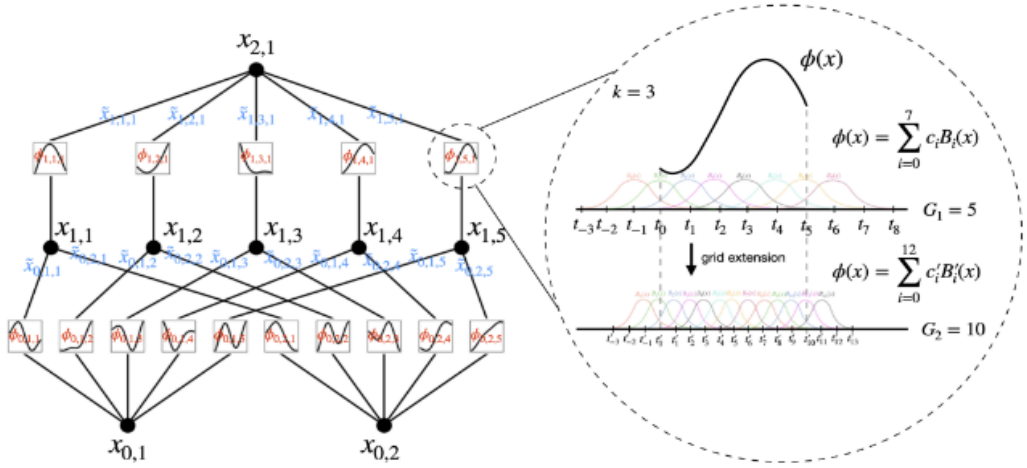

Fig. 1. KAN structure diagram.

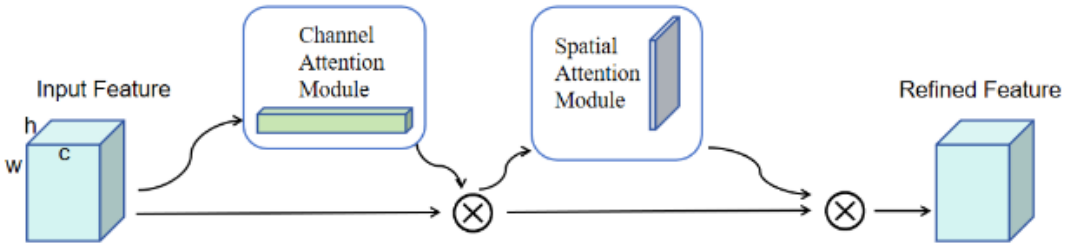

Fig. 2. CBAM architecture.

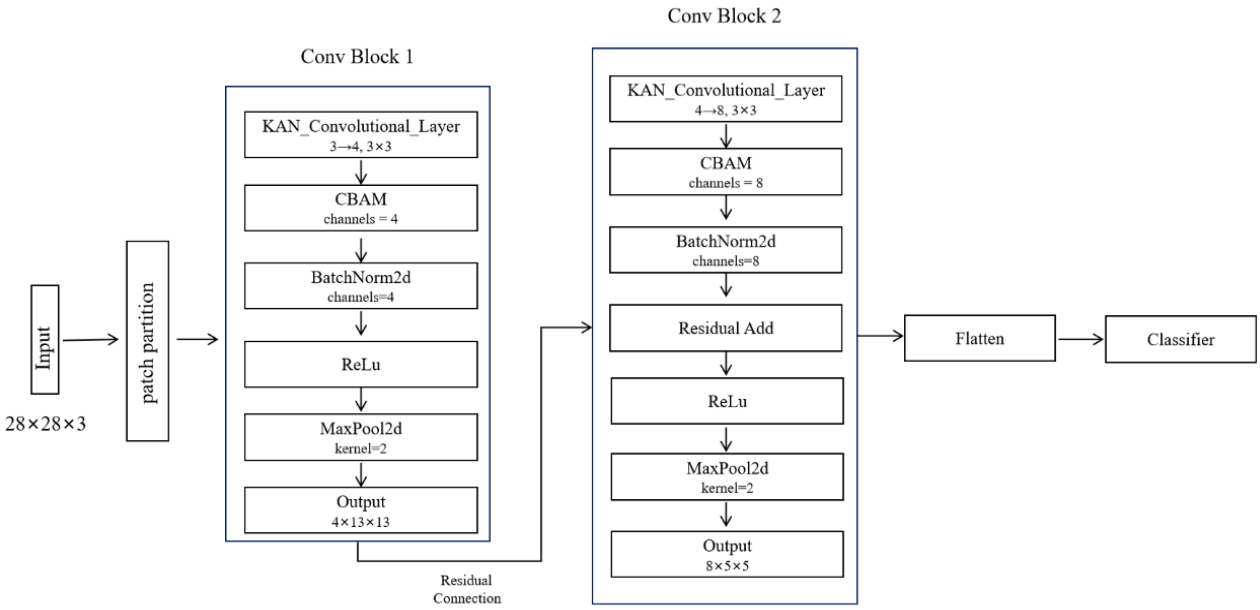

Fig. 3. Architecture of mammographic image classification model based on KAN-CBAM.

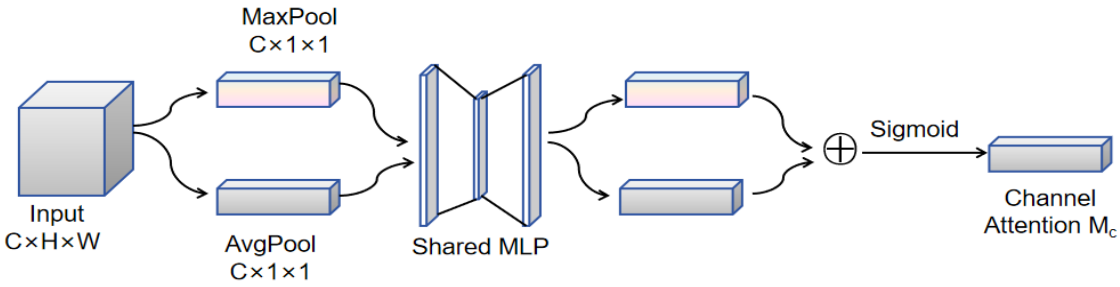

Fig. 4. CAM (Channel Attention Module).

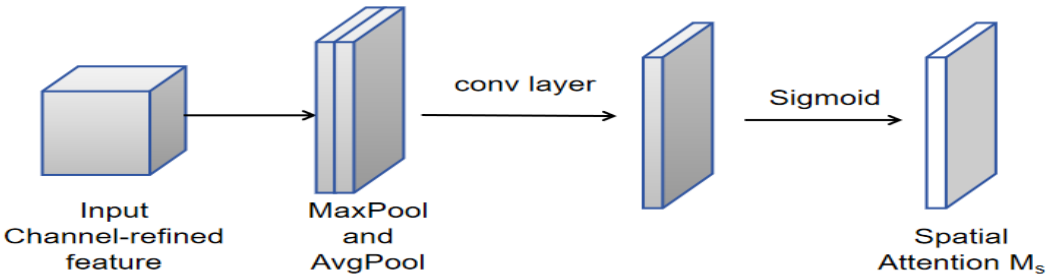

Fig. 5. SAM (Spatial Attention Module).

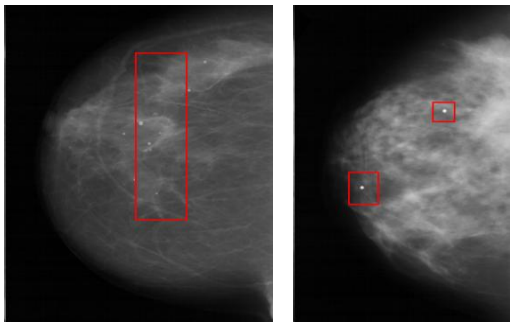

(a) Bright spots are easily misidentified as microcalcifications.

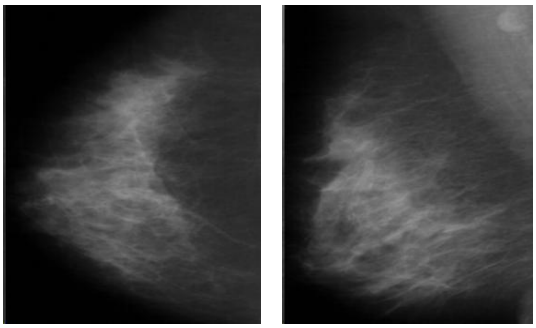

(b) The image resolution is relatively low.

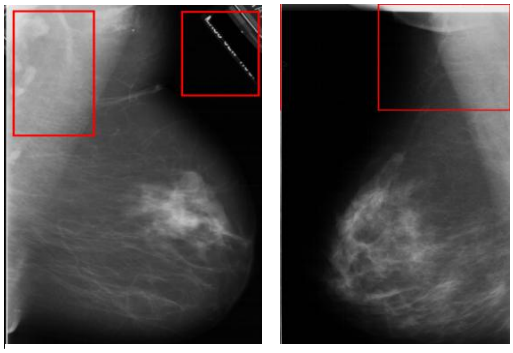

(c) Image noise interference.

Fig. 6. Dataset samples.

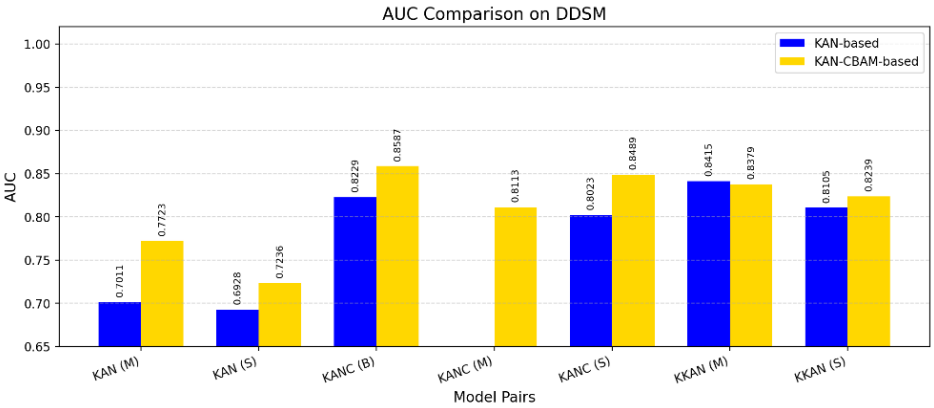

Fig. 7. AUC comparison of KAN-based and KAN-CBAM-based models for DDSM dataset.

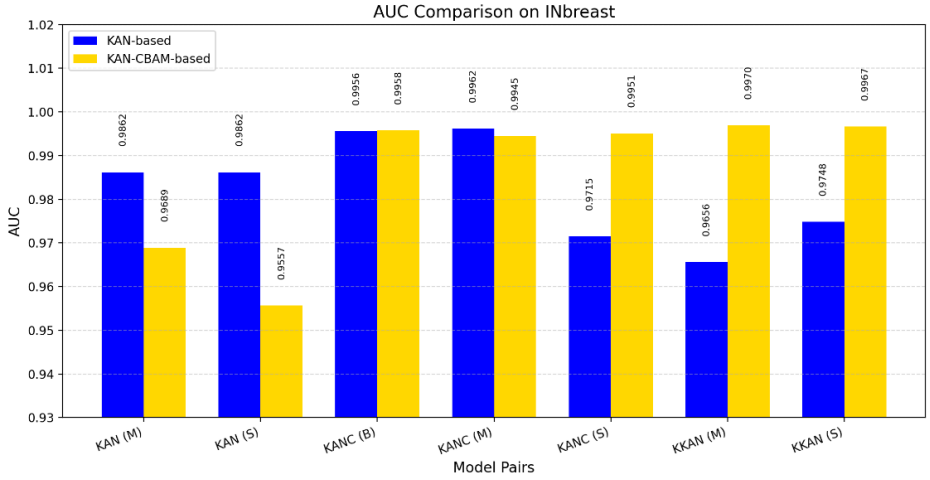

Fig. 8. AUC comparison of KAN-based and KAN-CBAM-based models for INbreast dataset.

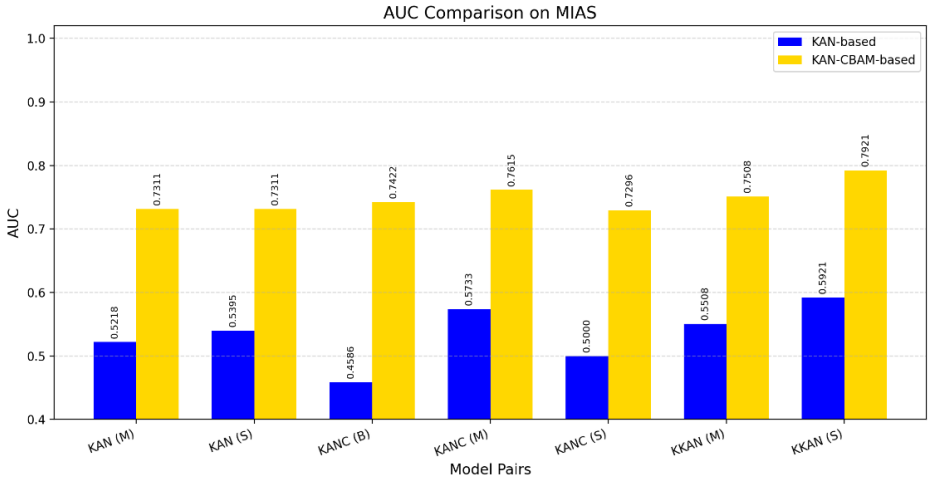

Fig. 9. AUC comparison of KAN-based and KAN-CBAM-based models for MIAS dataset.

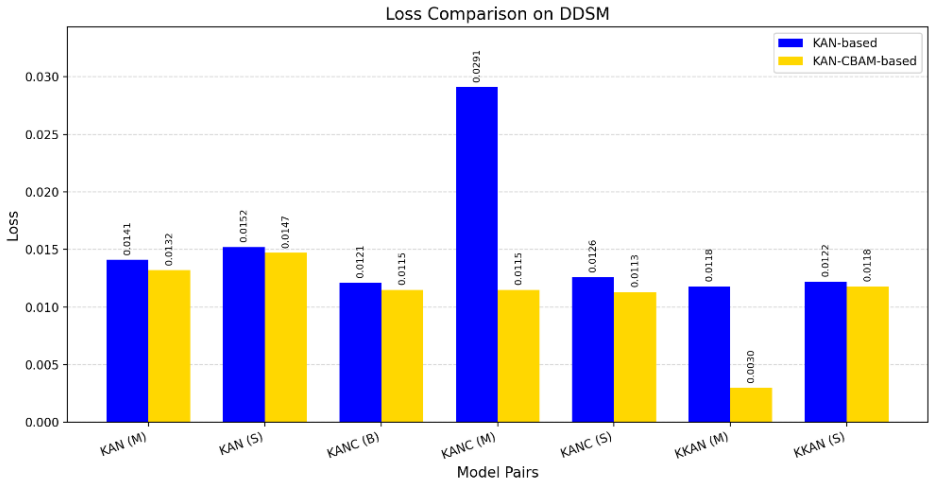

Fig. 10. Loss Comparison of KAN-based and KAN-CBAM-based models for DDSM dataset.

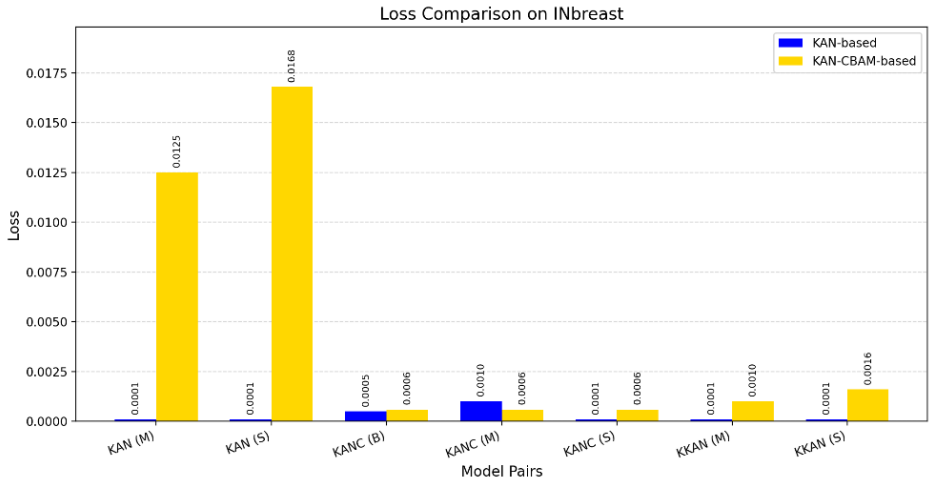

Fig. 11. Loss comparison of KAN-based and KAN-CBAM-based models for INbreast dataset.

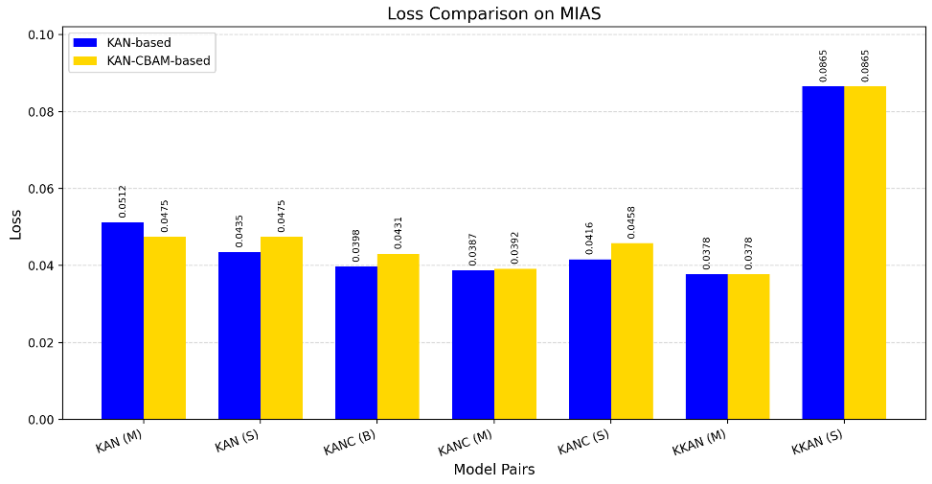

Fig. 12. Loss comparison of KAN-based and KAN-CBAM-based models for MIAS dataset.